Bulgarian Journal of Physics vol. **52** (2025) 221–236

Effect of Variation of Gravitational Coupling G on Geodesic Characteristics of the R-N based Black Hole Space-Time and Circular Orbit Stability

Indrajit Halder[1,2], **Kamal Lochan Mahanta**[2*], **Rakesh Ranjan Sahoo**[3]

[1]Department of Mathematics, Kanchrapara College, Kanchrapara, North 24 Parganas, West Bengal, India
[2]Department of Mathematics, C. V. Raman Global University, Bidyanagar, Mahura, Janla, Bhubaneswar, 752054, Odisha, India
[3]School of Basic Sciences & Humanities, Odisha University of Technology and Research, Techno Campus, Ghatikia, Bhubaneswar, 751029, Odisha, India
[*]Corresponding author Email: mahantakamal@gmail.com

Received: 10 December 2024
doi: https://doi.org/10.55318/bgjp.2025.52.3.221

Abstract. The Reissner-Nordström black hole has been studied extensively, but the consideration of variation of gravitational coupling G in the context of black hole solutions is less common. This study examines the geodesic paths of time-like and null particles near a black hole modeled on Reissner-Nordström (R-N), with particular attention to the role of gravitational coupling (G). The findings reveal that as particles move radially outward, both ordinary and proper time increase, reflecting a uniform and well-behaved spacetime. The research further explores the interplay between a particle's motion in the gravitational field of a black hole and the potential for stable orbits. Additionally, the stability of circular orbits is analyzed through the Lyapunov exponent.

KEY WORDS: Newtonian gravitational constant, Reissner-Nordström black hole, Geodesic, Effective Potential, Stability analysis.

1 Introduction

Black holes stand among the most enigmatic entities in astrophysics. They represent regions in spacetime from which nothing can escape. Typically, black holes are associated with spacetime singularities and event horizons. An event horizon is a boundary characterized by infinite redshift, effectively acting as a barrier that conceals physical information. The most basic description of a black hole involves three classical parameters: mass, angular momentum, and charge [1,2]. The Reissner–Nordström metric, a well-known solution attributable to Weyl,

Reissner, and Nordström in 1918, describes a static charged black hole, commonly referred to as the R-N metric. In this context, we examine the following black hole metric, grounded in the R-N black hole [3], incorporating G as the Newtonian gravitational constant.

$$ds^2 = -\Big(1 - \frac{2GM}{r} + \frac{GQ^2}{r^2}\Big)dt^2 + \Big(1 - \frac{2GM}{r} + \frac{GQ^2}{r^2}\Big)^{-1} dr^2 + r^2(d\theta^2 + \sin^2\theta d\phi^2)\,. \quad (1)$$

In this context, M and Q denote the mass and electro-magnetic charge of the black hole, respectively. Setting $G = 1$, the black hole metric (1) becomes the Reissner-Nordström (R-N) black hole. This serves as an electrically charged, spherically symmetric, and asymptotically flat solution to Einstein's field equations, delineating the spacetime geometry surrounding a spherically symmetric, non-rotating mass M with electric charge Q [4]. If we set $G = 1$ and take the limit $Q \to 0$, the metric reduces to the Schwarzschild metric. Conversely, as $G = 1$ with $Q \to \infty$, the spacetime geometry becomes asymptotically flat, trending towards the Minkowski metric [5]. An intriguing aspect of both theoretical and observational physics is the idea related to varying gravitational coupling. It is worth noting that cosmological models incorporating these changes in G are examined as alterations to the standard cosmological framework. Consequently, variations in G could potentially lead to significant impacts [6–9].
The motion of test particles and light along geodesic paths in gravitational fields provides significant insights into spacetime's geometry and dynamics. Specifically, examining the motion of null and radial geodesics is crucial for understanding how charged black holes, such as certain types of Reissner-Nordström or its de Sitter variant, interact with matter or radiation [10–13]. Numerous researchers [14–19] have utilized geodesic analysis to investigate the geodesic properties of various spacetimes. In this paper, we analyze the time-like and null geodesic behaviors of the black hole (1). Our detailed 'effective potential' diagrams demonstrate the potential for bound orbits, including circular and radial geodesics, designed with varying parameters. We also determine the energy and angular momentum of a test particle in the gravitational field of the black hole (1). This study has two main objectives: firstly, to evaluate the geodesic features of the black hole (1) spacetime under varying Newtonian gravitational constant G, and secondly, to assess the stability of circular orbits.

2 Geodesic Equation

The geodesic equation pertaining to the metric (1)

$$\frac{d^2x^i}{d\mu^2} + \Gamma^i_{jk}\frac{dx^j}{d\mu}\frac{dx^k}{d\mu} = 0\,. \quad (2)$$

In the equatorial plane, where $\theta = \frac{\pi}{2}$, the geodesics of spherically symmetric space-times, such as black holes, are typically articulated using the following equations from (1):

$$\begin{aligned} \frac{d\phi}{d\mu} &= \frac{J}{r^2}\,, \\ \frac{dt}{d\mu} &= \frac{e}{f(r)}\,, \\ \frac{dr}{d\mu} &= \sqrt{e^2 - (\frac{J^2}{r^2} + l) f(r)}\,, \end{aligned} \tag{3}$$

where e and J represent the energy per unit mass and angular momentum, respectively. In this context, l denotes the Lagrangian and

$$f(r) = \Big(1 - \frac{2GM}{r} + \frac{GQ^2}{r^2}\Big)\,.$$

For massless and massive particles, we take the values of l with 0 and 1 respectively. For a non-rotating black hole, we put J=0 in equations (3), and get

$$\frac{dr}{d\mu} = \sqrt{e^2 - l f(r)} \tag{4}$$

when the motion is purely in the radial direction, then we may express it as

$$\dot{r} \equiv \frac{dr}{d\mu} = \sqrt{e^2 - l f(r)} \tag{5}$$

and

$$\frac{dr}{dt} = \Big(1 - \frac{2GM}{r} + \frac{GQ^2}{r^2}\Big)\sqrt{1 - \frac{l}{e^2}\Big(1 - \frac{2GM}{r} + \frac{GQ^2}{r^2}\Big)}\,. \tag{6}$$

2.1 Null geodesic motion(l=0)

For the motion of a light-like particle along a null geodesic, setting $l = 0$ in equation (5) yields

$$\dot{r} \equiv \frac{dr}{d\mu} = e\,,$$

which yields the relationship

$$\pm e\mu = r\,. \tag{7}$$

In Figure 1(a), we present the plot based on the values of e specified within the illustration. Figure 1(a) illustrates the relationship (7) depicting how proper time (μ) varies with radial distance (r) in a spacetime framework. Furthermore,

by setting $l = 0$ in equation (6) for particles akin to photons, we derive the following:

$$\left(\frac{dr}{dt}\right)^2 = \left(1 - \frac{2GM}{r} + \frac{GQ^2}{r^2}\right)^2 .$$

Upon integrating this equation, we obtain

$$\pm t = \int \frac{dr}{1 - 2GM/r + GQ^2/r^2} . \tag{8}$$

Because the integrand in the integration process (8) is non-linear, the integration is quite complex. Therefore, we approximate $(2GM - GQ^2/r) \approx GQ^2/r$ within a specific vicinity of $1/r$ to retain the influence of G. By proceeding to

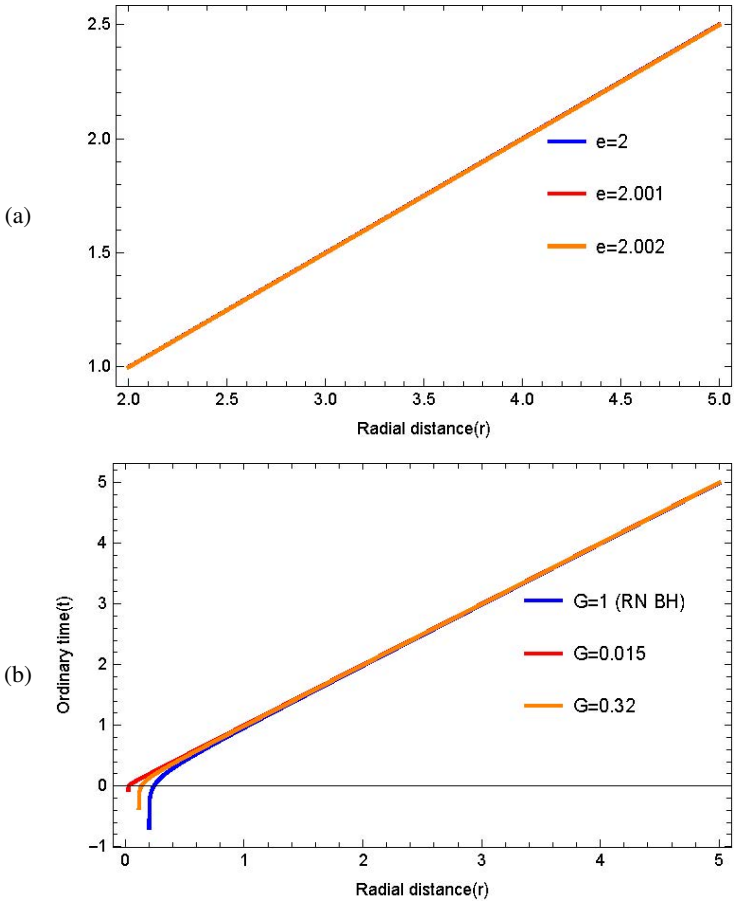

Figure 1. Variation of ordinary time and proper time w.r.t. radial distance.

integrate (8) under this assumption, we derive

$$\pm t = \int \frac{dr}{1 - GQ^2/r^2} \tag{9}$$

or,

$$\pm\, t \;= r + \frac{Q\sqrt{G}}{2} \ln \left| \frac{r - Q\sqrt{G}}{r + Q\sqrt{G}} \right| . \tag{10}$$

We have illustrated this relationship in Figure 1(b), setting $Q = 0.2$ and altering the values of G. Figure 1(b) depicts the relationship (10) between ordinary time (t) and radial distance (r) within a space-time geometry. The blue curve represents the RN-black hole. From the subfigures 1a and 1b, we note that varying G affects r in a similar manner for both proper time (μ) and ordinary time (t). For large distances from the black hole, space-time tends towards flatness. Figure 1 provides insight into the evolution of both the particle's proper time and ordinary time as it moves towards or away from the black hole. Consequently, the variation in the Newtonian gravitational constant G does not significantly influence the geodesic motion of a photon-like particle.

2.2 Timelike geodesic motion ($l = 1$)

In the case of a geodesic motion along a time-like path, setting $l = 1$ within equation (5), we derive

$$\dot{r} = \frac{dr}{d\mu} = \sqrt{e^2 - (1 - 2GM/r + GQ^2/r^2)}\,, \tag{11}$$

which yields

$$\pm\mu = \int \frac{dr}{\sqrt{e^2 - (1 - 2GM/r + GQ^2/r^2)}}\,. \tag{12}$$

Taking into account that $(2GM - GQ^2/r) \approx GQ^2/r$ within a specific vicinity of $1/r$, we then arrive at

$$\pm\mu = \int \frac{dr}{\sqrt{e^2 - 1 + GQ^2/r^2}}\,. \tag{13}$$

Integrating, we get

$$\pm\mu = \frac{1}{e^2 - 1} \sqrt{r^2\,(e^2 - 1) + GQ^2} \tag{14}$$

The relationship between proper time (μ) and distance (r) is depicted in Figure 2(a) using $e = 2$, $Q = 0.2$, while varying G values.

Substituting $l = 1$ into equation (6), we obtain

$$\frac{dr}{dt} = \left(1 - \frac{2GM}{r} + \frac{GQ^2}{r^2}\right)\sqrt{1 - \frac{1}{e^2}\left(1 - \frac{2GM}{r} + \frac{GQ^2}{r^2}\right)} \tag{15}$$

Assuming that within a specific vicinity of $1/r$, the expression $(2GM - GQ^2/r)$ is approximately equivalent to GQ^2/r, we derive

$$\frac{dr}{dt} = \left(1 - \frac{GQ^2}{r^2}\right)\sqrt{1 - \frac{1}{e^2}\left(1 - \frac{GQ^2}{r^2}\right)},$$

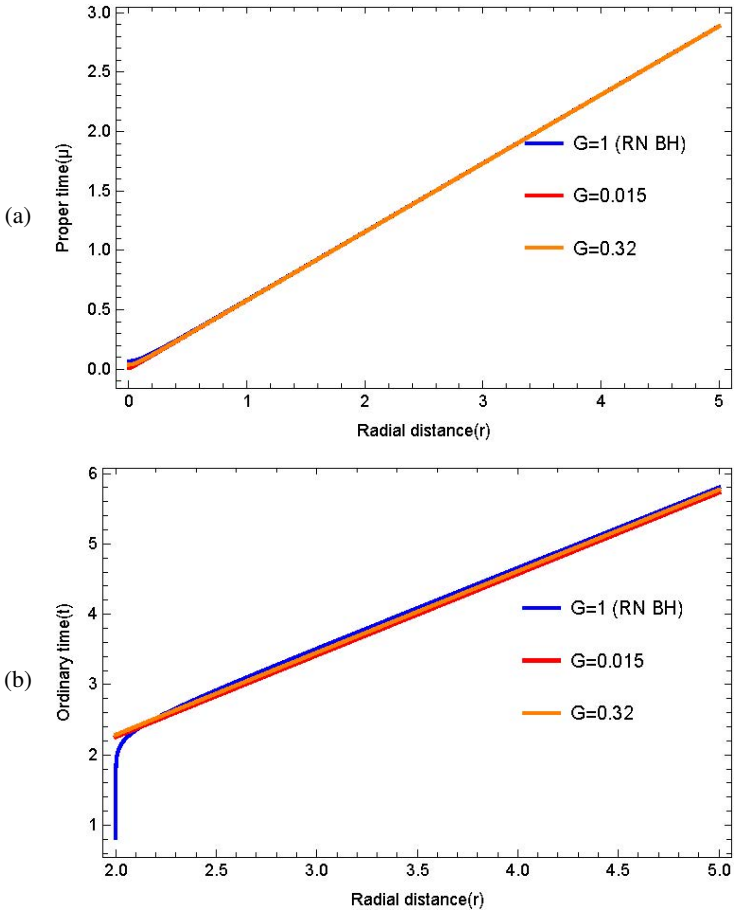

Figure 2. Variation of ordinary time and proper time w.r.t. radial distance.

which yields

$$\pm\, t = \int \frac{dr}{(1-GQ^2)/r^2)\sqrt{1-1/e^2(1-GQ^2/r^2)}} = \int \frac{r^3 dr}{(r^2-GQ^2)\sqrt{r^2\,(e^2-1)+GQ^2}}$$

Taking, $v^2 = \left(e^2-1\right) r^2 + GQ^2$, we obtain

$$\pm\, t \;= \frac{1}{e^2-1}\int \frac{\left(v^2-GQ^2\right) dv}{v^2-GQ^2e^2} = e.v + \frac{Q\sqrt{G}}{2}\ln\left|\frac{v-e.Q\sqrt{G}}{v+e.Q\sqrt{G}}\right|,$$

i.e.,

$$\pm\; t \;= \frac{e}{e^2-1}\sqrt{(e^2-1)\,r^2+GQ^2} + \frac{Q\sqrt{G}}{2}\ln\left|\frac{\sqrt{(e^2-1)\,r^2+GQ^2}-e.Q\sqrt{G}}{\sqrt{(e^2-1)\,r^2+GQ^2}+e.Q\sqrt{G}}\right|. \quad (16)$$

This provides the time (t)-distance (r) relationship, depicted in Figure 2(b), by setting $e = 2$, $Q = 0.2$, and adjusting the values of G. From the sub-figures in 2, it is evident that for different G values, the graphs of $r(\mu)$ and $r(t)$ closely resemble each other, especially when a particle is falling directly toward or away from the black hole. This resemblance illustrates the true trajectory of massive particles in curved spacetime. Consequently, it can be concluded that changes in the Newtonian gravitational constant G do not significantly affect the geodesic trajectory of the massive particle.

3 Effective Potential

When examining particle movement, particularly within black-hole spacetimes, the formulation of the effective potential serves as a crucial step. In our study, we derive the effective potential starting from our model. The effective potential V_{eff} is developed through a specific consideration [20–22]

$$V_{\text{eff}} = -\frac{1}{2}\left(\frac{dr}{d\mu}\right)^2 = -\frac{1}{2}\left[e^2 - \left(lf(r) + \frac{J^2}{r^2}f(r)\right)\right]. \quad (17)$$

3.1 V_{eff} in context of light-like test particle (l=0)

3.1.1 Case-(i) l=J=0

Considering a radial geodesic, we set $J = 0$ in equation (17), resulting in

$$V_{\text{eff}} = -\frac{1}{2}e^2\,.$$

Upon observing, we find that the effective potential becomes zero when the energy $e = 0$, indicating that the gravitational well does not influence the particle due to geodesic motion. Within these geodesics, it is solely related to the spacetime configuration, independent of the gravitational influence caused by the black hole's mass or charge.

3.1.2 Case-(ii) $l = 0, J \neq 0$

In circular motion, we may take $J \neq 0$, and put $l = 0$ in the equation (17), then we obtain

$$V_{\text{eff}} = -\frac{1}{2}e^2 + \left(1 - \frac{2GM}{r} + \frac{GQ^2}{r^2}\right)\frac{J^2}{2r^2} \tag{18}$$

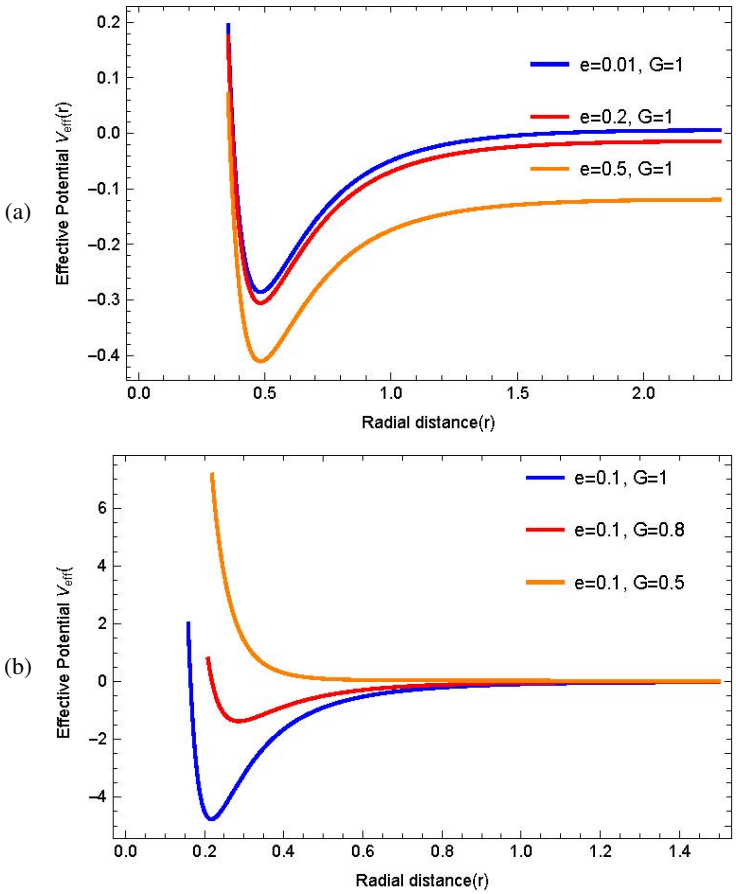

Figure 3. Effective potential for photon-like particle with $M = 1$, $J = 0.5$, $Q = 0.78$ & 0.55.

Utilizing equation (18), we generate the plot in Figure 3 which illustrates the effective potential function. The points where this curve intersects the radial axis indicate the horizon locations, and it is observed that V_{eff} remains negative between the two horizons, reaching a minimum value there, thus indicating stable circular orbits. In subfigure 3(a), it is clear that the distance between the outer and inner horizons widens as the energy e of a particle increases. Conversely, in subfigure 3(b), the blue graph represents the RN black hole, showing that a decrease in the value of G results in an increased effective potential, thereby narrowing the gap between the outer and inner horizons, potentially causing them to merge into a single horizon. Thus, fewer event horizons are noted with a reduction in G.

3.2 V_{eff} for massive test particle ($l = 1$)

For radial geodesics, setting $J = 0$ in equation (17) provides the effective potential as

$$V_{\text{eff}} = -\frac{1}{2}\left[e^2 - \left(1 - \frac{2GM}{r} + \frac{GQ^2}{r^2}\right)\right]. \tag{19}$$

3.2.1 Case-(i) When $e = 0$

Here, if we consider $e = 0$ in the equation (19), then V_{eff} becomes

$$V_{\text{eff}} = \frac{1}{2}\left(1 - \frac{2GM}{r} + \frac{GQ^2}{r^2}\right). \tag{20}$$

Next, input the value from equation (20) to graph the effective potential function depicted in Figure 4. Additionally, concerning radial geodesics, the angular momentum becomes zero, leading to the effective potential being zero at certain finite values of r. Similar to the prior scenario, we observe that the Newtonian gravitational constant G affects the black hole horizons, thereby allowing the possibility of a circular orbit.

(a)

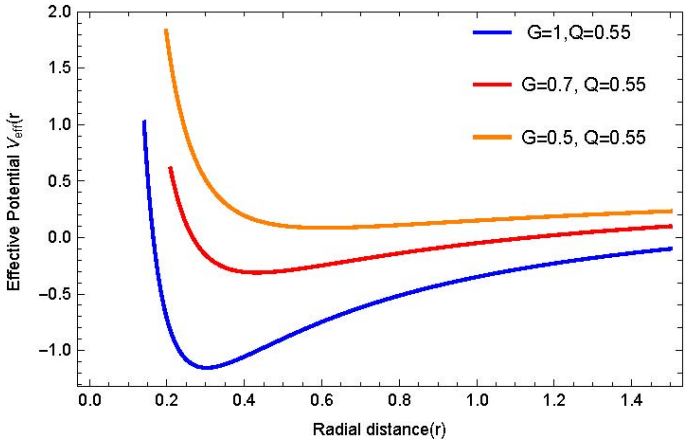

(b)

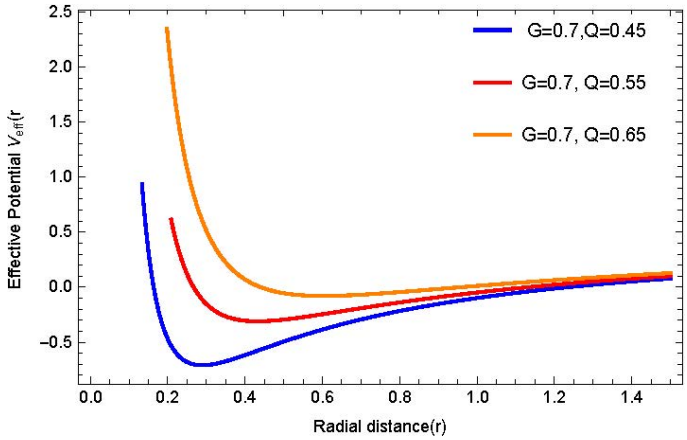

Figure 4. Effective potential for massive particle with $e = 0$ and $M = 1$.

3.2.2 Case-(ii) when $e \neq 0$

In this case, V_{eff} is

$$V_{\text{eff}} = \frac{1}{2}\left(-e^2 + 1 - \frac{2GM}{r} + \frac{GQ^2}{r^2}\right).$$

Here, where $e \neq 0$, the general representation of the effective potential function is depicted in Figure 5. Similar to prior cases, the Newtonian gravitational constant G significantly influences the black hole horizons, suggesting the potential presence of a circular orbit.

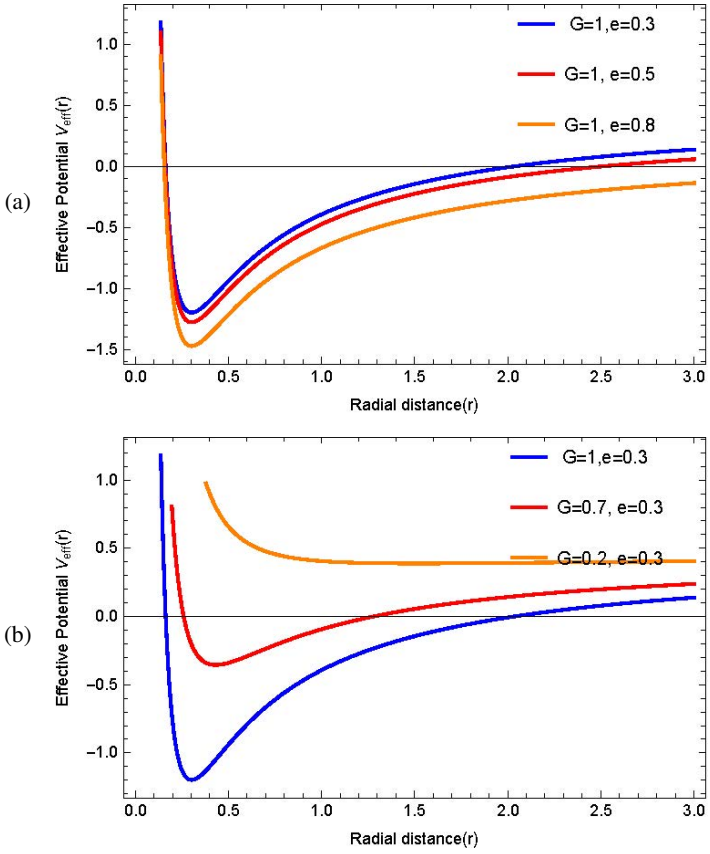

Figure 5. Effective potential for massive particle with $e \neq 0$ and $M = 1$.

4 Angular Momentum of Massive Particle Moving in Circular Orbit

Substituting $l = 1$ (massive particle) into equation (17), the effective potential is obtained as

$$V_{\text{eff}} = -\frac{1}{2}\left[e^2 - \left(1 + \frac{J^2}{r^2}\right) f(r)\right] .$$

For circular orbits, the following conditions apply

$$V_{\text{eff}} = 0 \quad \text{and} \quad \frac{dV_{\text{eff}}}{dr} = 0 ,$$

i.e.

$$-\frac{1}{2}\left[e^2 - \left(1 + \frac{J^2}{r^2}\right) f(r)\right] = 0 \tag{21}$$

and

$$\frac{1}{2}\left[\left(1 + \frac{J^2}{r^2}\right) f^{'}(r) - \frac{2J^2}{r^3} f(r)\right] = 0 . \tag{22}$$

Now, from these conditions (21) and (22), we have the following:

$$e^2 = \left(1 + \frac{J^2}{r^2}\right) f(r) \tag{23}$$

and,

$$J = \left[\frac{r^3 f'(r)}{2f(r) - rf'(r)}\right]^{1/2} \tag{24}$$

$$= r^{3/2}\left(\frac{2GM}{r^2} - \frac{2GQ^2}{r^3}\right)^{1/2} \times \left(2 - \frac{6GM}{r} + \frac{4GQ^2}{r^2}\right)^{-1/2} \tag{25}$$

Adjusting the value of G, we graph the forms obtained from equation (25) relative to angular momentum J. From the illustration in Figure 6, it's evident that angular momentum is influenced by the gravitational coupling G. There is a correlation where angular momentum rises alongside an increase in G. Consequently, G impacts the spin of the time-like particle within the gravitational vicinity of a black hole.

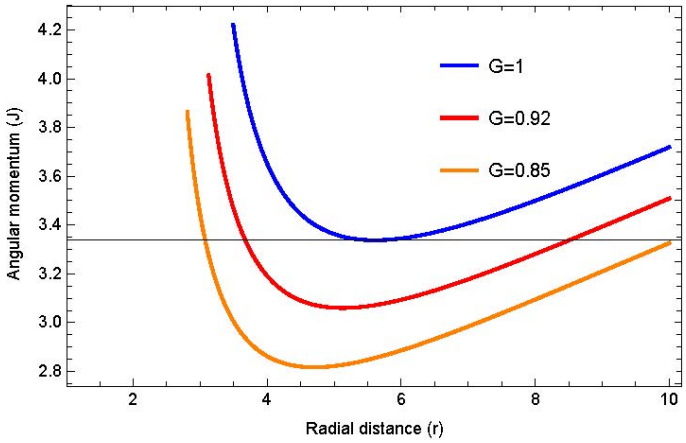

Figure 6. Variation of angular momentum.

5 Energy of Massive Test Particle Moving in Circular Orbit

Now, from equations (23) and (24), we have

$$e = \frac{\sqrt{2}f(r)}{\sqrt{2f(r) - rf'(r)}} = \frac{\sqrt{2}\left(1 - 2GM/r + GQ^2/r^2\right)}{\sqrt{(2 - 6GM/r + 4GQ^2/r^2)}}. \tag{26}$$

Utilizing equation (26), we illustrate the energy trajectories in Figure 7 while varying G. It is evident that the particle's energy experiences a greater increment with an increase in the value of G.

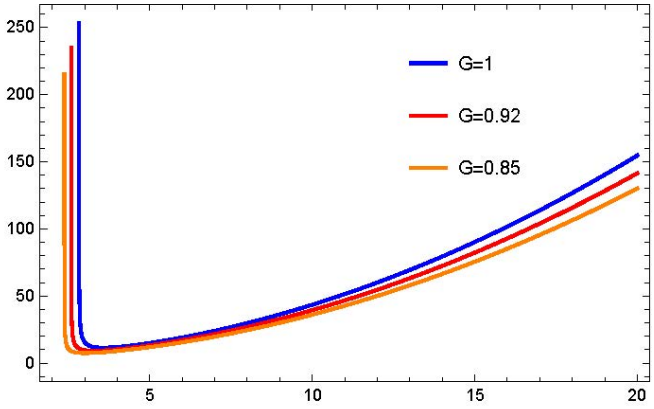

Figure 7. Variation of energy.

6 Stability of Circular Orbit of Massive Particle around Black Hole

In this section, we concentrate on the stability of circular orbits around black holes by analyzing how minor disturbances to these paths develop over time [24–26]. Our discussion centers on the stability of timelike particle orbits with respect to the Lyapunov exponent. Referring to Cardoso et al.'s work [23], we highlight the equation used to compute the Lyapunov component λ_l, which plays a crucial role in assessing orbital stability

$$\lambda_l = \sqrt{\frac{v''_{\text{eff}}}{2\dot{t}^2}}\,. \tag{27}$$

Here, t denotes coordinate time, and $\dot{t}$ is the derivative with respect to proper time, given by $\dot{t} = e/f(r)$ where $e = \sqrt{2}f(r)/\sqrt{2f(r) - rf'(r)}$. The orbit is considered chaotic or unstable when λ_l is real, and it is regarded as stable when the matrix possesses an imaginary λ_l.

Now,

$$\lambda_l^2 = \frac{v''_{\text{eff}}}{2\dot{t}^2} = \frac{v''_{\text{eff}}\,(2f(r) - rf'(r))}{4}\,.$$

From equation (19), we have

$$\begin{aligned}
V_{\text{eff}} &= \frac{1}{2}\Big(-e^2 + 1 - \frac{2GM}{r} + \frac{GQ^2}{r^2}\Big)\,,\\
\frac{dV_{\text{eff}}}{dr} &= \frac{1}{2}\Big(\frac{2GM}{r^2} - \frac{2GQ^2}{r^3}\Big)\,,\\
\frac{d^2V_{\text{eff}}}{dr^2} &= \frac{1}{2}\left(-\frac{4GM}{r^3} + \frac{6GQ^2}{r^4}\right)\,.
\end{aligned}$$

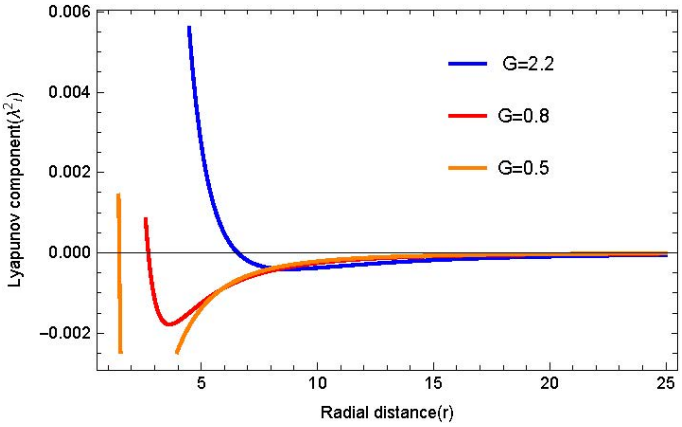

Figure 8. Variation of Lyapunov component (λ_l^2) with $M = 1$, $Q = 0.2$.

Now,

$$\lambda_l^2 = \frac{1}{4}\left[-\frac{2GM}{r^3} + \frac{3GQ^2}{r^4}\right]\left[2 - \frac{6MG}{r} + \frac{4GQ^2}{r^2}\right].$$

Simplifying, we have

$$\lambda_l^2 = \frac{1}{2}\left[-\frac{2GM}{r^3} + \frac{6G^2M^2 + 3GQ^2}{r^4} - \frac{13G^2Q^2M}{r^5} + \frac{6G^2Q^4}{r^6}\right] \tag{28}$$

As illustrated by equation (28), gravitational coupling plays a crucial role in determining the orbital stability of a time-like particle near a black hole. Figure 8 indicates that there exists a specific range of r where λ_l^2 is negative. Within this radial distance range (r), the massive particle can maintain a stable circular orbit around the black hole, provided the value of G remains within a certain lower threshold.

7 Conclusion

The research analyzes the trajectory of time-like and null particles near a Reissner-Nordström black hole, with an emphasis on gravitational coupling (G). It reveals that both regular and proper time grow as particles travel radially, indicating a uniform and smooth spacetime. This signifies a causal and ongoing interaction between particles and spacetime, where anticipated gravitational phenomena such as redshift and time dilation manifest, and the spacetime is devoid of singularities within the studied area. No significant effect of G was identified. For radial paths and photon-like particles, the effective potential becomes zero when energy is zero, making geodesics independent of the black hole's mass and charge. This implies that their motion is determined solely by spacetime structure rather than the gravitational pull of the black hole. This paper delves into the

behavior of non-radial and photon-like particles around black holes, emphasizing the traits of their potential functions. In particular, the potential is negative, exhibiting a minimum between two horizons and permitting stable circular orbits. It is noted that the gap between horizons widens with particle energy, while reducing the gravitational constant G elevates the effective potential, narrowing the gap and potentially converging the horizons. The paper also points out that radial geodesics with zero angular momentum display certain effective potential characteristics. Overall, the gravitational constant plays a pivotal role in defining black hole horizons and the feasibility of stable orbits. Additionally, the paper addresses how gravitational coupling correlates with the dynamics of a time-like particle in a black hole's gravitational realm, highlighting how angular momentum is influenced by gravitational coupling and rises with certain variables. It is also observed that energy escalates with changes to certain parameters. Gravitational coupling is key in sustaining stable orbits of time-like particles, evident within a particular range of radial distances when the coupling is sufficiently minor.

References

[1] R.A. Capobianco (2019) Geodesic motion in the Reissner-Nordström space-time. Doctoral dissertation. Universidade de São Paulo.

[2] J.B. Griffiths, J Podolský (2009) *Exact space-times in Einstein's general relativity*. Cambridge University Press.

[3] H. Reissner(1916) Über die Eigengravitation des elektrischen Feldes nach der Einsteinschen Theorie. *Ann. Phys. (Berlin)* **355**(9) 106-120.

[4] S. Antoci, D.E. Liebscher(2003) Editor's note: On the gravitational field of a mass point according to Einstein's theory by K. Schwarzschild. *Gen. Relativ. Gravit.* **35** 945-950.

[5] G. Nordström (1918) On the energy of the gravitation field in Einstein's theory. *Koninklijke Nederlandse Akademie van Wetenschappen Proceedings Series B Physical Sciences* **20** 1238-1245.

[6] J.P. Uzan (2003) The fundamental constants and their variation: observational and theoretical status. *Rev. Mod. Phys.* **75**(2) 403.

[7] J.D. Barrow (1998) Varying G and other constants. In *Current Topics in Astro fundamental Physics: Primordial Cosmology* . Dordrecht: Springer Netherlands, pp. 269-305.

[8] M. Toroš, M. Schut, P. Andriolo, S. Bose, A. Mazumdar (2024) Relativistic Dips in Entangling Power of Gravity. arXiv:2405.04661 [quant-ph].

[9] I. Halder, K.L. Mahanta, R.R. Sahoo (2024). Geodesic behavior of charged black hole in AdS spaces with Reissner–Nordstrom–AdS metric. *Can. J. Phys.* **103**(5) 426-436.

[10] E. Hackmann (2010) Geodesic equations in black hole space-times with cosmological constant. Doctoral dissertation, Universität Bremen.

[11] J.Louko, D. Marolf, S.F. Ross (2000) Geodesic propagators and black hole holography. *Phys. Rev. D* **62**(4) 044041.

[12] S. Fernando (2012) Schwarzschild black hole surrounded by quintessence: null geodesics. *Gen. Relativ. Gravit.* **44** 1857-1879.

[13] R.C. Rubio, F.D. Filippo, S. Liberati, M. Visser (2020) Geodesically complete black holes. *Phys. Rev. D* **101**(8) 084047.

[14] D. Abramson (2021) Geodesic Dynamics in Reissner-Nordström Geometry. *Thai J. Phys.* **38**(2) 69-98.

[15] S. Hajra (2022). An attempt of linking Maxwell with Newton to study gravitational phenomena. *Bulg. J. Phys.* **49**(4) 314.

[16] R. Zheleva (2024) Structure and astrophysics of self-gravitating objects in multi-scalar theories. *Bulg. Astron. J.* **41** 119.

[17] E. Guendelman, A. Kaganovich, E. Nissimov, S. Pacheva (2010) Nonsingular black holes from Gravity–Matter-Brane Lagranges. *Int. J. Mod. Phys. A* **25**(08) 1571-1596.

[18] L. Herrera, A.D. Prisco, J. Ospino, L. Witten (2020) Geodesics of the hyperbolically symmetric black hole. *Phys. Rev. D* **101**(6) 064071.

[19] I. Halder, K.L. Mahanta, R.R. Sahoo (2024) Geodesic Characteristics of the Black Hole in Bardeen AdS with Quintessence and Super-Radiant Effect. *Bulg. J. Phys.* **51**(3) 296.

[20] M. Kalam, N. Farhad, S.M. Hossein (2014) Geodesic study of a charged black hole. *Int. J. Theor. Phys.* **53** 339-349.

[21] M. Kalam, F. Rahaman, A. Ghosh, B. Raychaudhuri (2009) Discussion of some characteristics of charged Brane-world black holes. *Int. J. Mod. Phys. A 24*(04) 719-739.

[22] A. Romeo (1996) Black hole entropy and effective potential. *Class. Quantum Grav.* **13**(10) 2797.

[23] V. Cardoso, O.J.C. Dias (2004) Small Kerr–anti-de Sitter black holes are unstable. *Phys. Rev. D* **70**(8) 084011.

[24] R. Li, J. Zhao (2015) Numerical study of superradiant instability for charged stringy black hole–mirror system. *Phys. Lett. B* **740** 317-321.

[25] N.J. Cornish, J. Levin (2003) Lyapunov timescales and black hole binaries. *Class. Quantum Grav.* **20**(9) 1649.

[26] M. Mondal, P. Pradhan, F. Rahaman, I. Karar (2020). Geodesic stability and quasi normal modes via lyapunov exponent for hayward black hole. *Mod. Phys. Lett. A* **35**(30) 2050249.